

METHODS ARTICLE

Analyzing Biological Performance of 3D-Printed, Cell-Impregnated Hybrid Constructs for Cartilage Tissue Engineering

Zohreh Izadifar, MSc,¹ Tuanjie Chang, PhD,² William Kulyk, PhD,² Xiongbiao Chen, PhD,^{1,3} and B. Frank Eames, PhD^{1,2}

Three-dimensional (3D) bioprinting of hybrid constructs is a promising biofabrication method for cartilage tissue engineering because a synthetic polymer framework and cell-impregnated hydrogel provide structural and biological features of cartilage, respectively. During bioprinting, impregnated cells may be subjected to high temperatures (caused by the adjacent melted polymer) and process-induced mechanical forces, potentially compromising cell function. This study addresses these biofabrication issues, evaluating the heat distribution of printed polycaprolactone (PCL) strands and the rheological property and structural stability of alginate hydrogels at various temperatures and concentrations. The biocompatibility of parameters from these studies was tested by culturing 3D hybrid constructs bioprinted with primary cells from embryonic chick cartilage. During initial two-dimensional culture expansion of these primary cells, two morphologically and molecularly distinct cell populations (“rounded” and “fibroblastic”) were isolated. The biological performance of each population was evaluated in 3D hybrid constructs separately. The cell viability, proliferation, and cartilage differentiation were observed at high levels in hybrid constructs of both cell populations, confirming the validity of these 3D bioprinting parameters for effective cartilage tissue engineering. Statistically significant performance variations were observed, however, between the rounded and fibroblastic cell populations. Molecular and morphological data support the notion that such performance differences may be attributed to the relative differentiation state of rounded versus fibroblastic cells (i.e., differentiated chondrocytes vs. chondroprogenitors, respectively), which is a relevant issue for cell-based tissue engineering strategies. Taken together, our study demonstrates that bioprinting 3D hybrid constructs of PCL and cell-impregnated alginate hydrogel is a promising approach for cartilage tissue engineering.

Introduction

ALTHOUGH SIGNIFICANT PROGRESS has been made over the last few decades in developing tissue engineering strategies for cartilage repair,¹ regeneration of cartilage that functions similar to natural cartilage remains a challenging task. The exceptional biomechanical functionality of cartilage at the articulating surfaces of skeletal joints, in part, derives from the structural intricacies² and the biphasic (solid–liquid) nature of cartilage extracellular matrix (ECM).³ Resembling a reinforced highly hydrated material, cartilage ECM provides a favorable biological environment, so that impregnated chondrocytes can maintain tissue homeostasis, along with a noncompressible load-bearing function.^{4–7} A biomimetic cartilage tissue engineering approach creates scaffolds or constructs (i.e., cell-impregnated

scaffolds) with structural and biological functionality similar to cartilage. Tissue constructs that lack such structural and biologically conducive properties can result in an inferior performance, particularly after *in vivo* transplantation.^{8–10}

A hybrid cartilage tissue engineering strategy using both cell-impregnated hydrogels and polymeric scaffolds is emerging as an effective approach to mimic the biological and structural features of cartilage ECM. Hydrogels have many desirable properties for use in cartilage tissue engineering. They are highly hydrated and form tissue-like networks.¹¹ Furthermore, hydrogels are prepared easily, can be impregnated with cells, and provide an environment that is favorable for retaining the phenotype and morphology of chondrocytes.^{12,13} However, they have poor mechanical strength, which impairs their structural functionality for

¹Division of Biomedical Engineering, Department of ²Anatomy and Cell Biology and ³Mechanical Engineering, University of Saskatchewan, Saskatoon, Canada.

cartilage tissue engineering. Polymeric scaffolds, on the other hand, provide the required structural properties,^{14,15} but they are inferior to the hydrogels in terms of providing a biologically favorable, highly hydrated three-dimensional (3D) structure similar to natural cartilage matrix.⁸ Therefore, combining both hydrogel and polymeric components into a hybrid construct can mimic the biologically and structurally supportive properties of cartilage, offering promise for optimizing cartilage tissue engineering strategies.^{16–20}

Conventional hybrid constructs often lack reproducible and/or customized properties, due to limitations of the fabrication methods. Conventional approaches, such as free penetration or perfusion-assisted incorporation of hydrogel into scaffolds, do not allow customized cell seeding into the construct, which can affect negatively the distribution and organization of cells and, consequently, the quality of regenerated tissue matrix.^{15,17,19} For example, inefficient cell penetration into the scaffold can lead to formation of cartilage matrix only at the periphery of the construct.¹⁵ Indeed, lack of control over the spatial distribution of cells throughout the construct can lead to inferior matrix organization and function compared to that of natural cartilage.¹⁸ Advanced additive manufacturing techniques, such as three-dimensional (3D) bioprinting, can produce custom-designed, computer-controlled hybrid tissue constructs, overcoming many limitations of current biofabrication methods.^{21,22}

Three studies show the potential of 3D hybrid bioprinting as a superior fabrication technique for cartilage tissue engineering,^{23–25} but the biological performance of the impregnated cells has not been investigated comprehensively, and some critical fabrication parameters remain unexplored. Despite some positive results,²⁵ 3D hybrid bioprinting may decrease chondrocyte viability, due to thermal stresses from dispensing heated polymers adjacent to cell-impregnated alginate.²⁴ Increases in chondrocyte numbers and cartilage ECM production were observed in long-term culture of 3D hybrid constructs, but no images were presented²⁴ or little cartilaginous matrix was produced.²³ These studies leave open the question of whether this fabrication technique enables enough matrix production to replace the defective cartilage.

In addition, the amount of mechanical stresses that cells experience during biofabrication is determined by the viscosity of the alginate used.^{26,27} Alginate parameters meanwhile can influence long-term biological performance, such as proliferation and chondrogenic differentiation. For example, very high alginate concentrations resulted in lower biological performance,^{24,28,29} and very low alginate concentrations compromise the structural integrity of constructs.³⁰ Therefore, polycaprolactone (PCL) dispensing temperature and alginate rheological properties need to be carefully investigated, and the biological performance of impregnated cells, from viability to cartilage differentiation, should be evaluated qualitatively and quantitatively over long-term *in vitro* culture.

The success of engineered tissue constructs in promoting regeneration of cartilage is influenced largely by the type of employed cells.³¹ Primary chondrocytes and stem cells are the most investigated cell sources for cartilage tissue engineering.³² Since both cell sources offer advantages and disadvantages, there is still discussion and debate on which cell source is better suited for cartilage repair strategies. Primary chondrocytes more readily produce and maintain cartilage ECM, but they are obtained in low numbers from

donor cartilage and do not proliferate easily.^{33,34} Stem cells proliferate readily, but they have to be directed carefully toward chondrogenic differentiation.³⁵ Chondroprogenitors may represent a cell type intermediate to stem cells and chondrocytes, for they have the advantage of high expansion capability, while maintaining a predisposition to differentiate into chondrocytes.³⁶ Cartilage tissue engineering strategies can be optimized by investigating proliferation and differentiation of different cell types (e.g., chondrocytes vs. chondroprogenitors) in 3D biofabricated tissue constructs.

In this study, parameters of a 3D bioprinting technique, including thermal stress of melt-dispensed PCL and shear stress of dispensed alginate, were evaluated with respect to biocompatibility of hybrid cartilage constructs. The biological performance of hybrid constructs biofabricated with identified parameters of heat and alginate concentration/temperature were investigated during long-term *in vitro* culture using assays of cell survival, proliferation, and cartilage differentiation. To test whether the cell source influences the biological performance of these constructs, two morphologically distinct cell populations, rounded and fibroblastic, were isolated from primary cultures of embryonic chick chondrocytes. The biological performance of each population was very high, verifying the effectiveness of this cartilage tissue engineering approach. We discuss whether differences observed between these cell populations may reflect the differentiation state of the rounded versus fibroblastic cells.

Materials and Methods

Materials

LIVE/DEAD[®] Viability/Cytotoxicity Kit for mammalian cells (L-3224; Invitrogen), anti-collagen type II antibody [II-II6B3—Developmental Studies Hybridoma Bank (DSHB)], collagen type X antibody (X-AC9—DSHB), Goat anti-mouse IgG-488 conjugate (Millipore), RNeasy Mini Kit (Qiagen), RT² Easy First Strand Kit (Qiagen), SYBER master mix (Life Technologies), acetone (Fisher Scientific), methanol (Fisher Scientific), acetic acid (Fisher Scientific), and ethanol (Fisher Scientific). The rest of listed reagents and materials were purchased from Sigma-Aldrich. Polycaprolactone (PCL) (704105-Aldrich, Mw 48,000–90,000), alginate sodium salt; low viscosity alginate (LVA) (A2158-Sigma), alginate powder (AP) (180947-Aldrich), medium viscosity alginate (MVA) (A2033-Sigma), calcium chloride dehydrate (CaCl₂), Dulbecco's modified Eagle's medium (DMEM), Stemline[®] Keratinocyte Medium II-Calcium free (SKM), fetal bovine serum (FBS), phosphate buffer saline (PBS), phosphate buffer saline Tween-20 (PBST), HEPES buffer, collagenase type IA, trypsin, Hank's buffered salt solution (HBSS), antibiotic antimycotic (AA; containing penicillin, streptomycin, and amphotericin), kanamycin sulfate, glutamin, ascorbate acid, and sucrose. Ethylenediaminetetraacetic acid (EDTA), Alcian Blue, cacodylate buffer, sodium cacodylate, paraformaldehyde, glutaraldehyde, ruthenium (III) hexamine trichloride, normal goat serum, normal sheep serum, DMEM/F-12 Ham's medium, ascorbate-2-phosphate, insulin-transferrin-selenium (ITS).

Terminology

Due to variable usage of terms in the literature, we define how a few terms are used in this article. "Scaffold" will

refer to materials printed without cells, whereas “construct” will refer to materials printed with cells. “Hybrid scaffold” will refer to a structure printed with two materials (in this case, PCL and alginate), but no cells, while “hybrid construct” will refer to a structure with two materials as well as cells.

Design and fabrication of the hybrid constructs

Three-dimensional models of the hybrid constructs were designed to have porous nonwoven structure consisting of PCL framework scaffold and an embedded alginate hydrogel network in a box-shaped external geometry (Fig. 1A). The PCL and alginate strands were designed to have 1-mm spacing with 0/90° perpendicular pattern in two consecutive layers (Fig. 1A). The cell-impregnated alginate hydrogel was designed to be placed in the desired canals created between the PCL strands in each layer of the construct (Fig. 1C). The 3D computer-aided design (CAD) model of the hybrid construct was made using Magics Envisiontec (V13; Materialise) software. The 3D hybrid model was then sliced into consecutive multiple layers using Bioplotter RP (V2.9; Envisiontec GmbH) software, and loaded to the interface software (VisualMachine BP, V2.2; Envisiontec GmbH) of the 3D-Bioplotter™ system (Envisiontec GmbH) for construct fabrication (Fig. 1B), which was carried out in a sterile biosafety cabinet. PCL beads were loaded to a high-temperature dispensing head (HTDH), melted, and maintained at the desired temperature (65°C–80°C) for 15–20 min before dispensing. Dissolved alginate solution was loaded to a low-temperature dispensing head (LTDH) of the machine, maintained at 10°C for 10–20 min before dispensing. Following the CAD hybrid model, in each layer of the construct the PCL in the HTDH was first dispensed with the assigned pattern and then the alginate solution in LTDH was dispensed in the created canals between the PCL strands (Fig. 1C). This alternative dispensing pattern of PCL and alginate was repeated in subsequent layers to build the 3D hybrid constructs layer by layer as designed.

PCL was dispensed through a 300 μm metal cylindrical needle (24G) using a pneumatic pressure of 0.8 MPa at a dispensing speed of 1 mm/s. The alginate solution was dispensed through 200 μm conical needle, using 0.01 MPa pressure at a dispensing speed of 25 mm/s. Conical needles have been shown to be superior to cylindrical needles in

dispensing live cells with lower shear-induced cell damage.³⁷ Since alginate gelation improves its stability and structural integrity,³⁸ a partial cross-linking process was adopted throughout the construct fabrication. 170 mM CaCl₂ aerosol was produced with an ultrasonic nebulizer (MY-520) and was applied externally to the dispensing alginate, which takes about 10 s for each layer. Such partial cross-linking also keeps the construct moist and prevents it from drying during the fabrication. The partial cross-linking was followed by a 20 min full cross-linking of the finished 3D hybrid construct in 100 mM CaCl₂ solution to gel the alginate network within the PCL scaffold.

Characterization of hybrid scaffold fabrication

Different parameters of the fabrication process, such as material characteristics and processing conditions, were investigated to ensure the biocompatibility of the hybrid biofabrication for encapsulating cells. To identify a suitable processing temperature of PCL, scaffolds were made at different PCL temperatures (65°C, 70°C, 75°C, and 80°C) using a pressure of 0.8 MPa, and the heat distribution on the surface of dispensing PCL strands was monitored with an infrared thermal camera (FLIR i3; FLIR systems, Inc.). Upon dispensing of a 10-mm-long PCL strand, infrared (IR) images were collected for analysis. Surface temperature profile along the length of the dispensed PCL strand was measured in the collected IR images using FLIR ThermoCAM Researcher Software (FLIR systems, Inc.). Before collecting images, the infrared thermal camera was calibrated with an ice–water mixture (0°C).

Three different sodium alginate stocks; namely, AP, LVA, and MVA, were used for preparing alginate solutions (dissolving in dH₂O) and testing the fabrication of the hybrid scaffold. The effect of temperature on the viscosity of alginate solution (2% w/w) was investigated using a programmable rheometer (Brookfield DV-III Ultra). The alginate temperature was decreased from 25°C–26°C to 10°C by two degrees at a time and its viscosity was measured. At each temperature, at least 10 min wait time was given for the material to uniformly reach the desired temperature before viscosity was measured. The effect of temperature on the viscosity of higher concentrations of LVA solution (4% and 5%) was also investigated for comparison.

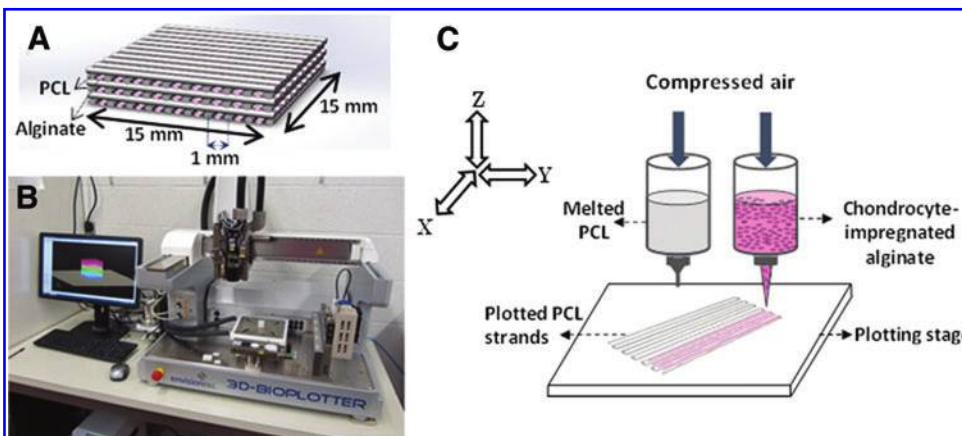


FIG. 1. Design and three-dimensional (3D) bioprinting of hybrid constructs with structural and biological features. (A) Schematic of designed 3D hybrid construct with alternating strands of polycaprolactone (PCL) and chondrocyte-impregnated alginate in each layer, (B) 3D-Bioplotter™ system employed for biofabrication of designed hybrid constructs, and (C) hybrid biofabrication using pneumatic dispenser heads. Color images available online at www.liebertpub.com/tec

Cell isolation and culture

All experiments were carried out according to approved institutional and national standards of animal ethics. Primary chondrocytes were isolated from cartilaginous sternums of 14-day-old chick embryos. Embryonic chick cartilage was used as the cells source because of the easy accessibility of large numbers of cartilage-producing cells, and it is a well-characterized model for studying the development and differentiation of cartilage cells in different culture conditions^{39–43} and tissue scaffolds.^{44–47} Since monolayer passaging of the primary chondrocytes can negatively affect their chondrogenic differentiation capacity,^{48,49} 20 to 24 embryos were used to obtain sufficient numbers of primary cells without needing to passage them (i.e., passage 0). The excised sternums of chick embryos were finely chopped and subsequently subjected to digestion in 0.2% collagenase and 0.25% trypsin in HBSS at 37°C and 5% CO₂ for 2 h with one gentle pipetting at 90 min. The digestion was stopped by adding DMEM and 10% FBS to the digestion medium. The resulting cell suspension was passed through a sterile Nitex (70 µm mesh size) and centrifuged at 200 g for 10 min. The collected cell pellets were suspended in a culture medium containing DMEM, 10% FBS, 2 mM glutamine, 0.1 mg/mL kanamycin, 1% AA (100 U/mL penicillin, 0.1 mg/mL streptomycin, 0.25 µg/mL amphotericin B), and 0.01 mg/mL ascorbate. The isolated cells were seeded at a population of 2×10^6 cells/flask (T-75 flask; VWR) at 37°C and 5% CO₂ and the medium was changed every 3 days. Of note, the culture medium used for 3D culture of cells in constructs did not contain additional growth factors, which are not needed for primary cells from embryonic cartilage to differentiate as chondrocytes,^{50–53} perhaps due to the self-expression of chondrogenic growth factors by these embryonic cells.⁵⁴

Two morphologically distinct cell types, rounded and fibroblastic, were observed in the primary cultures after 7 days of two-dimensional (2D) culture *in vitro* (see Results section and Fig. 4). Rounded and fibroblastic cells were collected separately from the culture at day 10 following the primary isolation. To collect rounded cells, the culture medium was gently pipetted up and down twice to dissociate any loosely attached round cells. Then, the floated and dissociated cells were harvested and centrifuged at 300 g for 10 min to pellet the cells. The remaining fibroblastic cells attached to the culture flasks were rinsed with PBS and incubated with 0.25% trypsin solution at 37°C for 5 min. Following the incubation, the FBS-containing culture medium (described earlier) was added to the flask to neutralize the trypsin. The flask medium was gently pipetted up and down to disperse detached cell clumps, which was then centrifuged at 300 g for 10 min to pellet the cells. Cell number and viability in the collected rounded and fibroblastic cell suspensions were determined using a hemocytometer and Trypan blue exclusion assay, respectively.

Biofabrication of cell-impregnated hybrid construct

MVA solution (3.5% w/w) was prepared by stir-bar mixing of alginate sodium salt in the Stemline Keratinocyte Medium under sterile condition. For each cell type, the alginate solution was evenly mixed with cells suspended in a fresh culture medium (7:3, alginate volume:cell-

suspension volume) using three-way stopcocks to a final alginate solution concentration of 2.5% and cell concentration of 5.68×10^6 cells/mL. The cell-embedded alginate was then loaded to the LTDH of the 3D Bioplotter machine and the 3D PCL-alginate constructs with impregnated cells were dispensed following the hybrid fabrication procedure described earlier. During the biofabrication, the temperature of the plotting stage was maintained at 10°C. After cross-linking of the finished cell-embedded hybrid constructs in 100 mM CaCl₂ in 4.2 mM HEPES and 0.35 M sucrose solution (pH7.4), the constructs were washed in DMEM twice for 5 min each, and were moved to 12-well culture plates containing DMEM supplemented with 10% FBS, 2 mM glutamine, 0.1 mg/mL kanamycin, 0.01 mg/mL ascorbate, and 100 U/mL penicillin, 0.1 mg/mL streptomycin, and 0.25 µg/mL amphotericin B. The hybrid constructs were maintained at 37°C and 5% CO₂ condition with a fresh medium change every 3 days.

For biological studies, hybrid constructs with two consecutive layers were fabricated and used. Furthermore, to better approximate the thickness of human articular cartilage (1.5–2.35 mm⁵⁵), multilayer hybrid constructs with six consecutive layers were designed and fabricated using cells of the ATDC5 cell line previously employed for cartilage tissue engineering applications.^{56,57} ATDC5 mouse cells were purchased from Sigma and cultured in culture flasks containing the DMEM/F-12 HAM's medium supplemented with 5% FBS, penicillin (100 U/mL), streptomycin (100 µg/mL), glutamine (2 mM), ascorbate-2-phosphate (0.05 mg/mL), and 1X ITS+. The medium was changed every 2 days. Confluent cells after 1 week of culture were collected, re-suspended in the serum-free DMEM/F-12 HAM's medium, and mixed with alginate (5.6×10^6 cells/mL in 2.5% alginate solution) for construct biofabrication following the procedure described earlier. The hybrid 6-layer constructs were then maintained at 37°C and 5% CO₂ condition with a fresh medium change every 3 days.

Cell viability and proliferation assay

The cell viability assay was conducted in the hybrid constructs using the two-color LIVE/DEAD Kit and fluorescence microscopy. Green-fluorescent calcein-AM dye staining certifies live cells with a normal intracellular esterase activity, whereas red-fluorescent ethidium homodimer-1 (EthD-1) dye staining identifies dead cells with compromised plasma membranes. The viability of cells in the hybrid constructs was assayed immediately after biofabrication (day 0), and at days 1, 3, 7, and 14 of subsequent *in vitro* culture. At each time point, the constructs ($n=3$) were removed from the culture, washed with DMEM, and stained in 2 µM calcein-AM and 0.5 µM EthD-1 solution in DMEM for 30 min in a 37°C, 5% CO₂ incubator. The constructs were washed with DMEM twice and imaged using a fluorescence microscope (Nikon, ECLIPSE E600, SPOT Insight™ Camera).

Sequential images at different vertical focal planes were captured to investigate the spatial distribution and viability of the impregnated cells within the hydrogel. To quantitatively determine the cell viability in the hybrid constructs, the stained cells were released from the constructs by dissolving hydrogel matrix with 50 mM EDTA solution (diluted in DMEM) for 30 min at room temperature, while

protected from light. Using gentle pipetting, the medium was dispersed to give an even cell suspension mixture. Samples ($N=3$) were taken from the cell mixture of each construct and imaged under a coverslip on a standard glass microscope slide at five to six random locations for counting live and dead cells. The cell number in these isolated cell suspensions ($n=3$) was determined using a hemocytometer to indicate proliferation over the culture period. The cell viability and proliferation experiment was repeated thrice in independent experiments, and the collected data were used for quantitative viability and proliferation analysis.

Cell differentiation assessments

Cartilage differentiation of the cells was investigated by assaying glycosaminoglycans (GAGs) and collagen deposition in the hybrid constructs. Alcian blue staining was used to assay sulfated GAGs at days 1, 7, 14, and 28 following biofabrication. At each time point, the constructs ($n=3$) were removed from the culture and washed twice with DMEM. The constructs were fixed in acetone and methanol solution (1:1) on ice for 30 min and then stained with 0.5% Alcian blue diluted in 3% acetic acid solution (pH=1) overnight. The stained constructs were washed once with 25% ethanol in 3% acetic acid and once with 50% ethanol in 3% acetic acid and were then imaged using light microscopy. Using ImageJ software,⁵⁸ the amount of Alcian blue-stained matrix in the hybrid constructs was estimated by measuring the percentage area of the blue-stained matrix to the total field of view in the alginate of the constructs at days 7, 14, and 28 of culture.

Immunofluorescent staining was performed to detect Col2 or Col10 accumulation within the hybrid constructs. The constructs were harvested at days 1, 7, and 14 following biofabrication, washed with DMEM, and fixed in the cacodylate buffer (200 mM sodium cacodylate (pH7.4), 20 mM CaCl_2 , 4% sucrose) containing 2% paraformaldehyde, 2% glutaraldehyde, and 0.7% ruthenium (III) hexamine trichloride for 2 h at 4°C on a shaking platform. The constructs were then washed once in the cacodylate buffer, digested with 0.5% trypsin in PBS for 20 min at 37°C for antigen retrieval, and then incubated in a blocking buffer (4% normal goat serum and 2% normal sheep serum in PBST) for 2 h while shaking at room temperature. The constructs were then incubated in purified anti-Col2 or anti-Col10 antibody in a blocking buffer (1:100) overnight at 4°C while shaking. Next, the constructs were washed six to eight times with the blocking buffer over 2 h and then incubated with goat anti-mouse IgG-488 conjugate in the blocking buffer (1:1000) at 4°C overnight. Constructs were then washed in PBST for at least 2 h before fluorescence microscopy imaging. Histochemical and Immunofluorescent staining experiments were repeated twice in independent experiments to confirm the obtained results.

Relative levels of Collagen type I alpha 2 (*Col1a2*) and Collagen type II alpha 1 (*Col2a1*) transcript expression in cells harvested from the hybrid constructs were investigated using quantitative polymerase chain reaction (qPCR) analysis following manufacturer's protocols. At day 0, rounded and fibroblastic cells were released from hybrid constructs, using the same procedure described earlier for cell viability and proliferation assays, and total RNA was extracted using

the RNeasy Mini Kit (Qiagen). For each sample, 100 ng of RNA was reverse transcribed into cDNA using the RT² Easy First Strand Kit (Qiagen). qPCR was performed in 20 μL of reaction volume using 1 μL of cDNA products, gene-specific primers, and SYBR master mix with 46 cycles of denaturation (30 s, 95°C), annealing (30 s, 55°C), and extension (30 s, 72°C) using a Stratagene™ Mx3005P qPCR system (Agilent Technologies, Inc.). Primer sets for chick *Col2a1* (Forward: aagggtgatcgtggtgagac, Reverse: tcgcctctgtctcctgttt), *Col1a2* (Forward: tgaagttggctttgatgcag, Reverse: ggggtcttttggagccttc), and internal reference *Hprt1* (Forward: aagtgccagttgttggc, Reverse: ttgtagtcgagggcgatcc) were synthesized by IDT. The PCR efficiency was measured as 102% that was in the acceptable range of 95–110%. Ratio changes in gene expression were calculated using the $\Delta\Delta\text{Ct}$ method.^{59,60}

Statistical analysis of the data

Collected data are presented as mean \pm standard deviation. Statistically significant difference among different time points and cell types was calculated using one-way or two-way analysis of variance (ANOVA) and Tukey's multiple comparison test. Differences were significant when the calculated p -value was less than 0.05.

Results

Investigating parameters of hybrid construct fabrication for biocompatibility and structural integrity

To assess the level of potential heat stress on cells in adjacent alginate strands during hybrid construct fabrication (Fig. 1), the surface temperature of printed PCL strands was determined using an infrared camera. Although the PCL was dispensed at 65°C–80°C, the surface temperature of the PCL strands dropped considerably once printed (Fig. 2). The temperature profiles along the 10-mm length of printed PCL (x axis and marked black line in Fig. 2 inset images) indicate that the PCL surface temperature dropped to room temperature (25°C) within approximately 10 s after printing at 1 mm/s. When PCL was printed at 65°C, 70°C, 75°C, and 80°C, the maximum temperature at the surface of the printed PCL was 33.9°C, 38.1°C, 39°C, and 42.4°C, respectively (Fig. 2), which was almost half the applied processing temperatures. Since cells are cultured at 37°C, PCL temperatures of 65°C–75°C should allow biocompatible printing of hybrid constructs with impregnated cells. Because of the lower viscosity and higher flow rate of PCL at higher temperatures, 75°C PCL printing was used for all subsequent experiments of this study.

Stability of the alginate strands during printing is important for maintaining the designed structural properties of the hybrid construct. To identify parameters by which the stability of low-concentration alginate could be controlled effectively, alginate viscosity was characterized as functions of temperature, concentration, and the polymer chain length of starting material. At 2% concentration, MVA exhibited significantly ($p<0.001$) higher viscosity than the low-viscosity alginates, LVA and AP, at every temperature tested between 25°C and 10°C (Fig. 3). A similar statistically significance ($p<0.001$) increase in viscosity was achieved by increasing the concentration of LVA from 2% to 5%

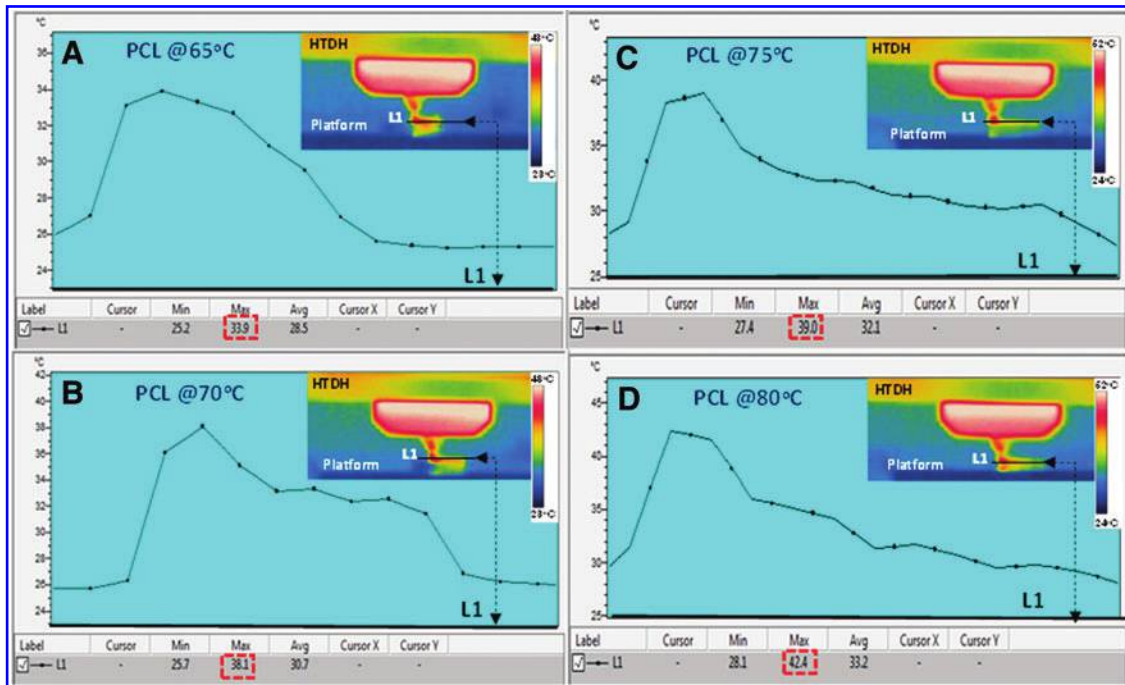


FIG. 2. Thermal infrared (IR) imaging reveals that temperature decreases rapidly during PCL strand printing. Surface temperature profile along the length of printed PCL (L1 in the *inset* images) shows a rapid drop to ambient temperature after printing at (A) 65°C, (B) 70°C, (C) 75°C, or (D) 80°C. *x* axes in the graphs corresponds to the *black line* (L1) marked along the length of printed PCL in the *inset* IR images. HTDH: high-temperature dispensing head. (The heat map scale bar was created automatically from the detected range of temperatures in each captured field of view). Color images available online at www.liebertpub.com/tec

(Fig. 3). Lowering the temperature from 25°C to 10°C significantly ($p < 0.001$) increased the alginate viscosity at all concentrations tested. However, the viscosity increase in 2% MVA and 4% and 5% LVA was three to eight times larger than that in 2% LVA and 2% AP (Fig. 3), which was statistically significant ($p < 0.001$). At 2% and 2.5% concentrations, printing of hybrid constructs with low-viscosity

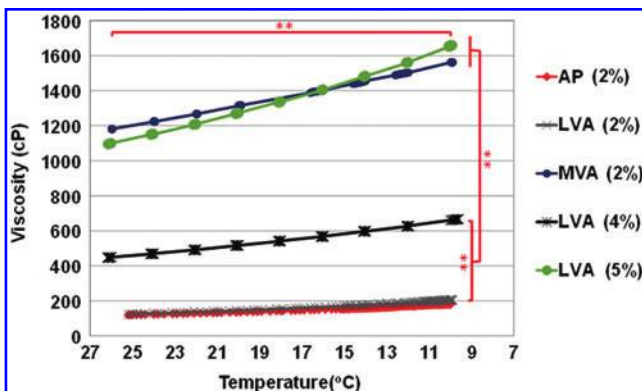


FIG. 3. Increase of viscosity by temperature decrease in solutions of low viscosity alginate (LVA), medium viscosity alginate (MVA), and alginate powder (AP). Asterisks indicate statistically significant difference in viscosity from 25°C to 10°C for all tested solutions (*horizontal asterisks*) and at every tested temperature between 2% MVA and 5% LVA and 2% LVA, 2% AP and 4% LVA at $p < 0.001$. Color images available online at www.liebertpub.com/tec

alginate (LVA and AP) was found to be very challenging, even by lowering the alginate temperature and employing partial cross-linking with CaCl_2 aerosol during fabrication. LVAs did not have enough stability to maintain their 3D structures, and the alginate strands flattened after printing (data not shown). However, hybrid constructs printed with 2% and 2.5% MVA at 10°C maintained their structural integrity (Fig. 6). As such, a higher initial viscosity of alginate along with printing at a low temperature can provide a processing condition for making stable hybrid constructs with low alginate concentrations, which is an alternative and more biocompatible approach than using high alginate concentrations.

Two populations of primary cells were isolated from embryonic chick cartilage

Two morphologically distinct cell types, rounded and fibroblastic, were observed in primary cultures of embryonic chick sternal chondrocytes after 7 days of 2D culture *in vitro* (Fig. 4). Rounded cells with spherical morphology floated in the culture medium or were attached loosely to the flask bottom (Fig. 4B, C, white arrowheads). Fibroblastic cells with flattened morphology were attached firmly to the flask bottom and could not be detached by simple pipetting (Fig. 4B, C, blue arrowheads). Interestingly, fibroblastic cells appeared to give rise to rounded cells when cultured after the floated and loosely attached rounded cells were removed (Fig. 4D–F).

In addition to the morphological differences between rounded and fibroblastic cells, molecular analyses indicated

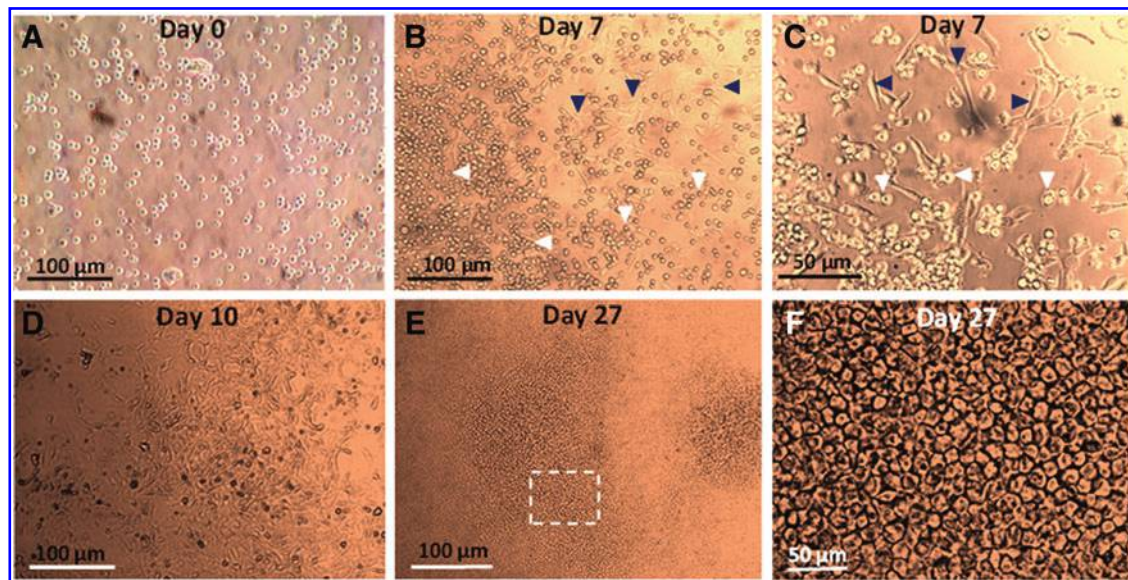


FIG. 4. Two populations of cells were isolated from primary chick cartilage. Primary cells isolated from embryonic chick cartilage in 2D culture at (A) day 0 and (B, C) day 7. (C) is higher magnification view of sample in (B). *Dark blue arrowheads* point to fibroblastic cells, and *white arrowheads* point to rounded cells. (D) 2D culture at day 10 following removal of floated and loosely attached rounded cells. (E, F) Many rounded cells appeared by day 27, 17 days after removal of floated and loosely attached rounded cells. (F) shows higher magnification view of *dashed box* in (E). Color images available online at www.liebertpub.com/tec

they had different gene expression profiles. Quantitative gene expression analysis using qPCR was performed to further investigate the difference between the rounded and fibroblastic cells. At day 0, immediately after biofabrication, rounded cells were observed to have statistically higher *Col2a1* mRNA levels than the fibroblastic cells, while fibroblastic cells were observed to have statistically higher *Col1a2* mRNA levels than the rounded cells (Fig. 5). Given these morphological and molecular differences, the biological performance of rounded and fibroblastic cell populations in 3D hybrid constructs was evaluated separately.

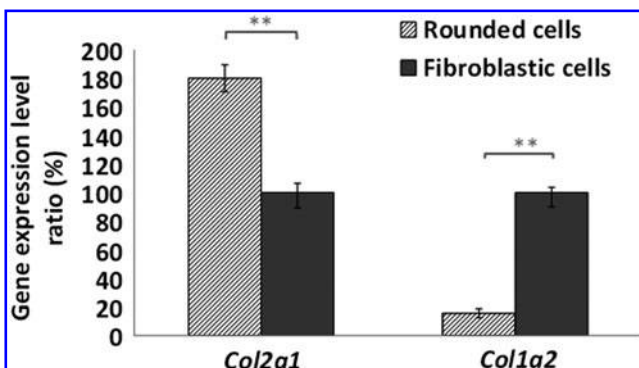


FIG. 5. Rounded cells have distinct molecular characteristics from fibroblastic cells. Quantitative polymerase chain reaction analyses revealed higher levels of *Col1a2* and lower levels of *Col2a1* expression in fibroblastic cells than rounded cells at day 0 of hybrid construct biofabrication. Levels of *Col2a1* and *Col1a2* mRNAs are normalized with respect to those in fibroblastic cells. *Asterisks* indicate $p < 0.001$.

Rounded and fibroblastic cells demonstrated high viability in hybrid constructs

Biocompatibility of the PCL temperature and alginate processing parameters identified above was measured using a fluorescent cell viability assay. After 3D hybrid construct printing (day 0), cells were observed to be distributed uniformly, without formation of cell clumps, throughout the alginate strands between the PCL strands (Fig. 6). Fluorescent imaging of stained constructs at day 0 showed uniform distribution of both live and dead cells throughout the alginate portion of the constructs immediately after printing (Fig. 7). The absence of increased cell death in regions of alginate that were immediately adjacent to the PCL strands confirms that the heat produced by melt-dispensed PCL does not harm considerably the viability of impregnated cells (Fig. 7A–F). No differences in the distribution of cells were observed between rounded and fibroblastic cells.

Time-course analysis indicated that both rounded and fibroblastic cells maintained high viability in hybrid constructs cultured *in vitro*. At day 0, constructs with rounded and fibroblastic cells both showed a cell viability of more than 80% (Fig. 7G). The cell viability of constructs containing fibroblastic cells decreased to 76% by day 7, which was improved to about 85% by day 14 (Fig. 7G), although these changes were not statistically significant. For constructs with rounded cells, the viability remained high (>80%) throughout the 14 days of culture, slightly increasing from days 3 to 14 (Fig. 7G), although not statistically significant. From days 1 to 14 during culture, rounded cells tended to exhibit slightly higher viability than fibroblastic cells, but this was only statistically significant on day 7 (Fig. 7G). In general, the cell viability was high in hybrid constructs of both cell types, with a minimum viability of 77%.

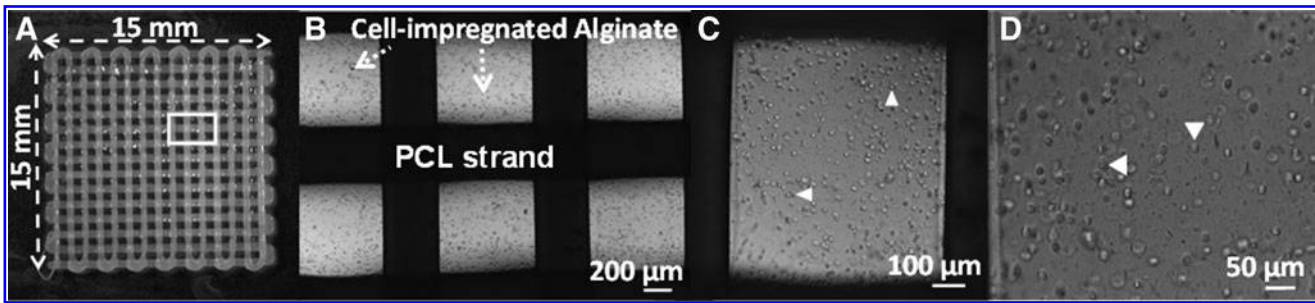


FIG. 6. 3D bioprinted hybrid constructs have uniformly distributed impregnated cells within the alginate hydrogel. (A) Gross and (B–D) magnified light microscopy views. (B) is higher magnification view of the box in (A). Dashed arrows point to cell-impregnated alginate strands, and white arrowheads point to cells impregnated in the alginate strand.

Fibroblastic cells had higher proliferation than rounded cells in hybrid constructs

To ensure that the hybrid construct provided a stable environment for cell proliferation during *in vitro* culture, cell number, cell organization, and the structural integrity of alginate were examined. Representative images of hybrid constructs (Fig. 8A–F) suggested that the number of live rounded and fibroblastic cells increased during culture. Quantitative analyses of the number of rounded and fibroblastic cells suggested that hybrid constructs provide a conducive environment for maintaining cell proliferation (Fig. 8I). Cell numbers steadily rose during the culture pe-

riod for both rounded and fibroblastic cells, each showing a significant increase in cell number at day 14 compared to earlier culture times. Rounded and fibroblastic cells exhibited similar cell numbers at each time point during culture up to day 7, but at day 14, fibroblastic cells had significantly higher numbers (3.7-fold increase) than the rounded cells (2.5-fold increase) (Fig. 8I).

Cell proliferation was associated with the formation of cell clusters during *in vitro* culture of hybrid constructs. Most cells were dispersed individually throughout the alginate strands at day 1, but at later time points, discernible cell clusters became apparent (inset images in Fig. 8A–F). A high-resolution (0.83 μm pixel size) confocal image of the

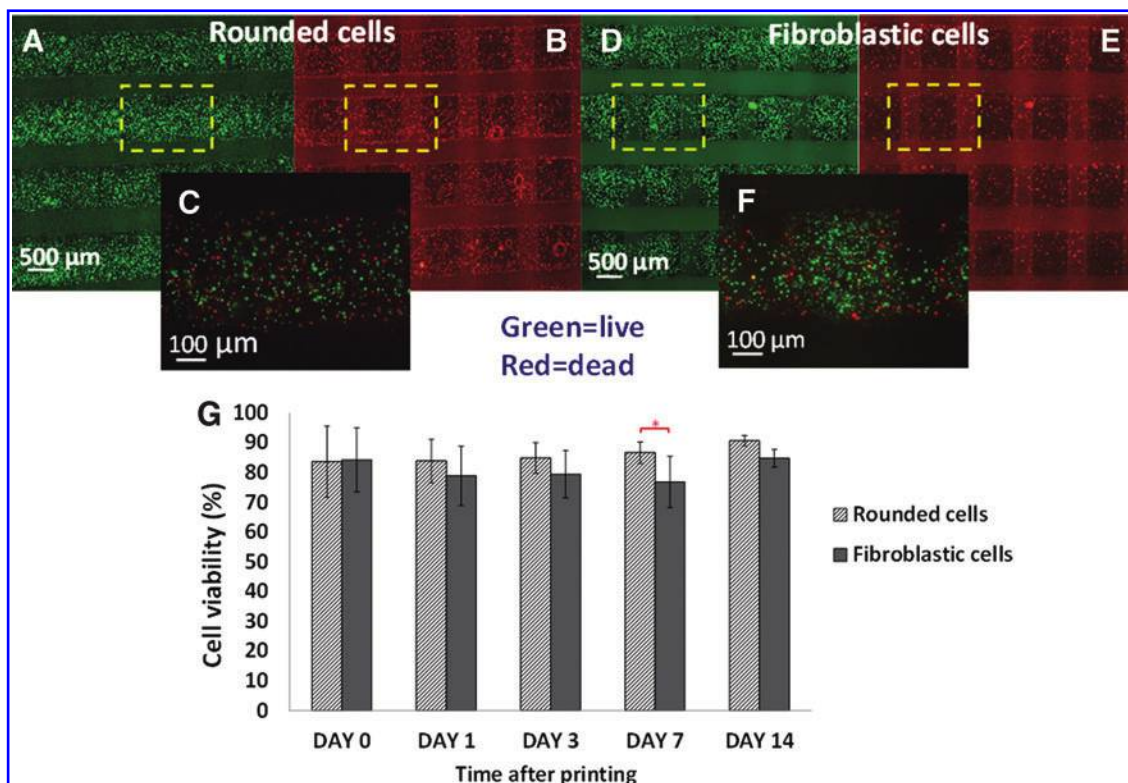


FIG. 7. Cell viability was high for both rounded and fibroblastic cells in 3D bioprinted hybrid constructs. Uniform distribution of (A) live, (B) dead, and (C) live and dead rounded cells, and (D) live, (E) dead, and (F) live and dead fibroblastic cells in hybrid constructs confirms the harmless use of melted PCL in hybrid fabrication. (G) Time course cell viability analysis demonstrates high viability for rounded and fibroblastic cells in the hybrid constructs. Asterisk indicates a statistical significant difference with $p < 0.05$. Color images available online at www.liebertpub.com/tec

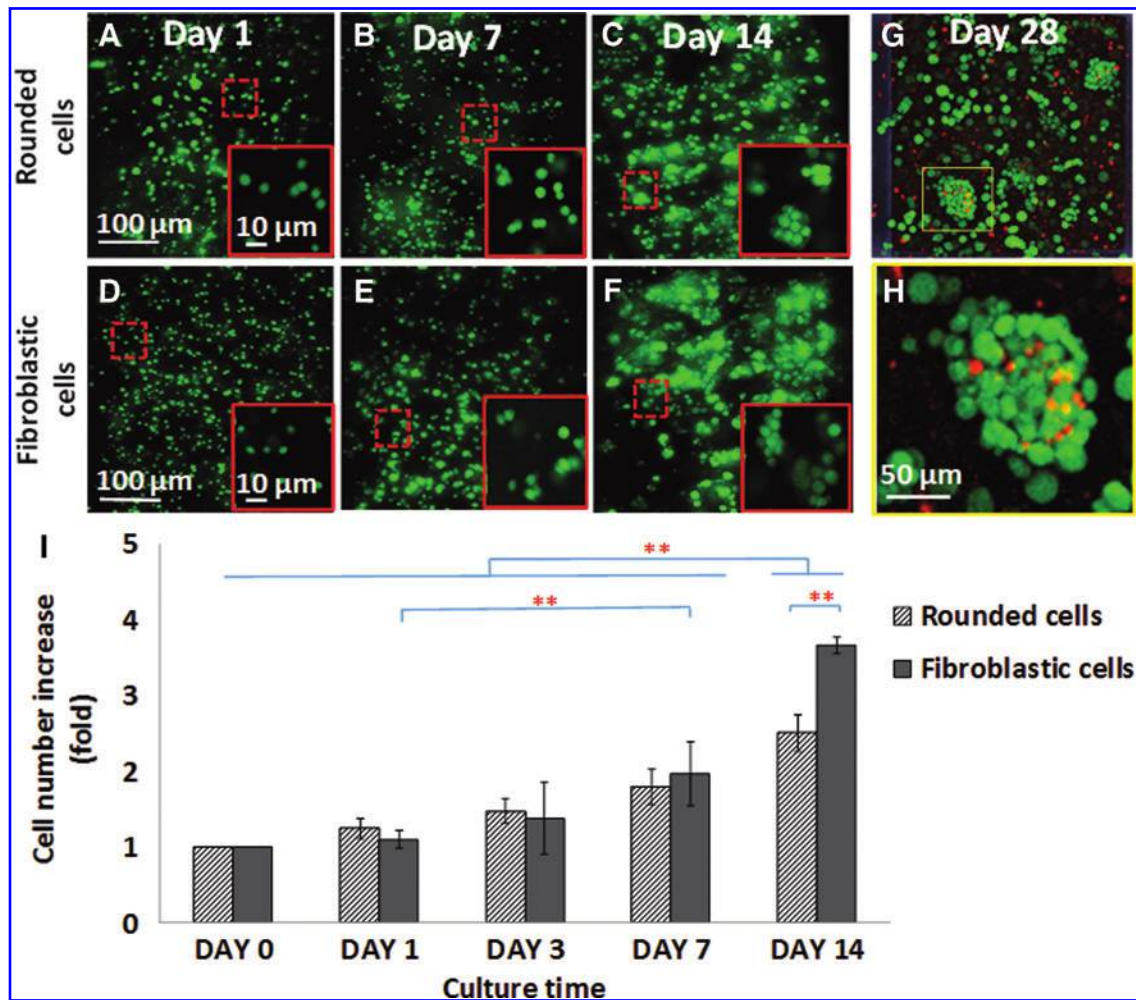


FIG. 8. Qualitative and quantitative cell proliferation analyses indicate cell population increases in hybrid constructs with time in culture. Live-stained constructs impregnated with rounded (A–C) and fibroblastic cells (D–F) at day 1 (A, D), day 7 (B, E), and day 14 (C, F). (G, H) Confocal image of *green* and *red* stained rounded cells in a hybrid construct at day 28 of culture. *Inset* images and (H) are high magnification view of the cells in the constructs showing cell cluster formation in hybrid constructs over time. (I) Fold increases in cell numbers in hybrid constructs over time. *Asterisks* indicate statistically significant difference with $p < 0.001$. Color images available online at www.liebertpub.com/tec

rounded cell hybrid construct taken at day 28 of culture revealed that most cells were in clusters rather than isolated (Fig. 8G, H). In addition, both rounded and fibroblastic cells displayed round morphologies that typify chondrocytes in native cartilage during *in vitro* culture of hybrid constructs (inset images in Fig. 8A–F).

Throughout *in vitro* culture, the alginate strands retained both external and internal structural integrity. Alginate strands persisted in filling the space between PCL strands, maintaining the interconnectivity of pores within the hybrid constructs during 28 days of culture (Fig. 8A–G). At later times of culture (such as day 28), the size of alginate strands sometimes appeared to increase (data not shown), perhaps due to osmotic swelling of the alginate or a gradual loosening of the internal microstructure of the hydrogel matrix. In contrast to this latter possibility, cells within the alginate strands displayed the same uniform distribution as seen after initial fabrication, suggesting that the internal structure of alginate was preserved during *in vitro* culture.

Rounded and fibroblastic cells secrete abundant cartilage matrix within hybrid constructs

Abundant Alcian blue and Col2 immunofluorescence staining reflected secretion of the two main components of cartilage tissue matrix, GAGs and Col2,⁶¹ within hybrid constructs during *in vitro* culture. Alcian blue staining was localized around cells in the alginate hydrogel of the hybrid constructs from both rounded and fibroblastic cells (Fig. 9A–L). Over the culture time points, regions of Alcian blue-stained matrix appeared to increase in size within both the rounded and fibroblastic cell hybrid constructs. At days 7 and 14, fibroblastic cells seemed to produce more Alcian blue-stained matrix than the rounded cells (Fig. 9C, D, I, J). At day 28, the Alcian blue-stained matrix almost filled the alginate strands of the hybrid constructs for both rounded and fibroblastic cells (Fig. 9E, F, K, L).

To quantitate these observations, the relative area of Alcian blue-positive matrix was measured at each time point during the culture period, and these measurements confirmed the

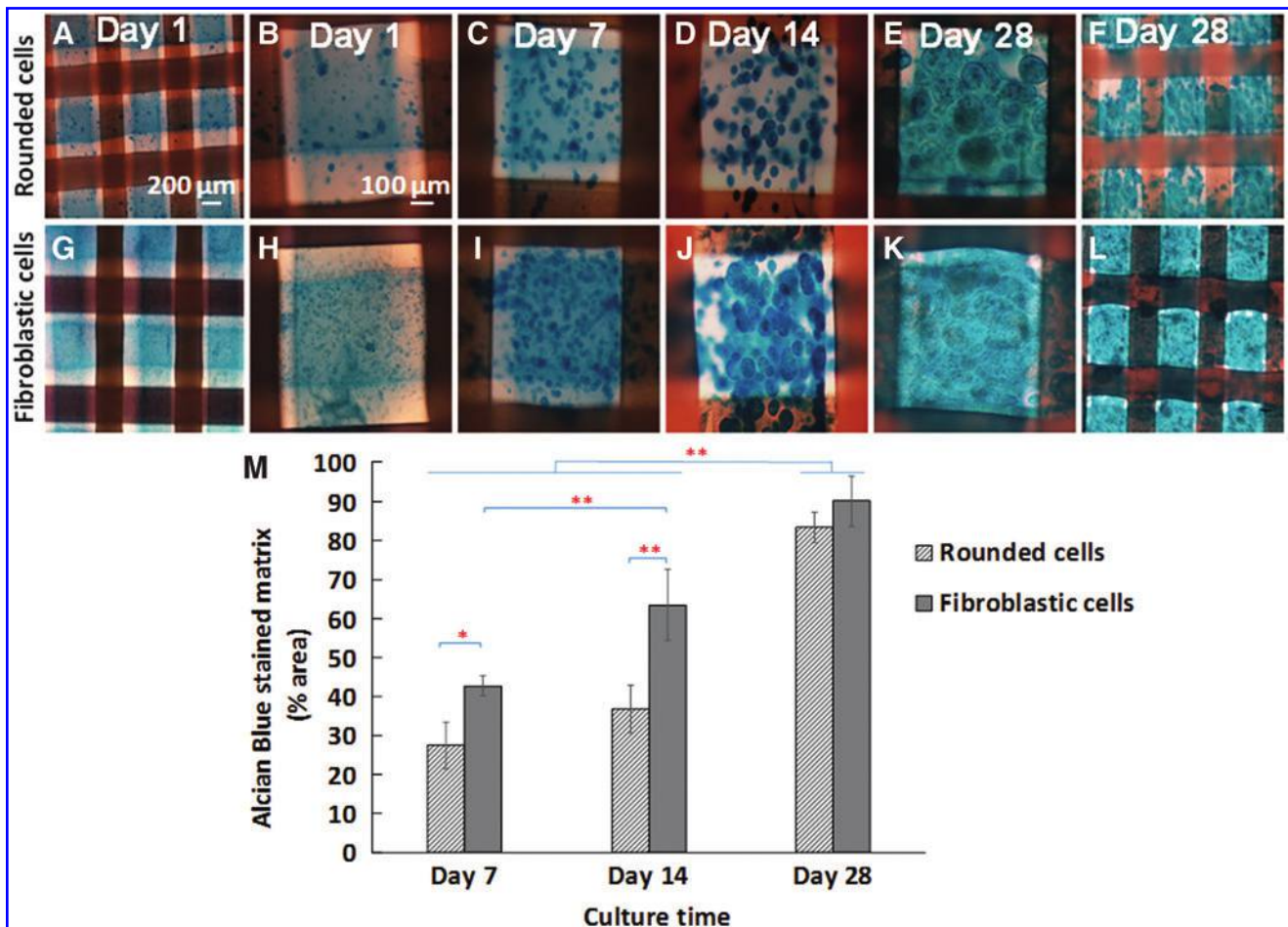


FIG. 9. Increased secretion of Alcian *blue*-positive matrix in the 3D hybrid constructs over *in vitro* culture time. Alcian *blue*-stained 3D constructs impregnated with (A–F) rounded and (G–L) fibroblastic cells at day 1 (A, B, G, H), day 7 (C, D), day 14 (D, J), and day 28 (E, F, K, L). (B, E, H, K) are high-magnification views of samples in (A, F, G, L), respectively. (M) Quantitative increase of Alcian *blue*-positive matrix in 3D hybrid constructs over time in culture for rounded and fibroblastic cells. *Single asterisk* and *double asterisks* indicate statistically significant differences with $p < 0.05$ and $p < 0.001$, respectively. Color images available online at www.liebertpub.com/tec

trends observed in the images. Reflecting GAG secretion, Alcian blue-stained matrix increased over culture time for both rounded and fibroblastic cells, being significantly higher at day 28 compared to days 7 and 14 (Fig. 9M). Alcian blue-stained matrix significantly increased at day 14 compared to day 7 for fibroblastic cells. At each time point measured, fibroblastic cells showed larger regions of Alcian blue-stained matrix than rounded cells, with statistical significance at days 7 and 14. Alcian blue-stained matrix accounted for more than 80% of the measured area of alginate strands by day 28 in both rounded and fibroblastic cell constructs (Fig. 9M). In total, these data confirm that hybrid constructs provide a favorable environment for increased secretion of cartilaginous matrix during long culture periods.

Col2 immunostaining demonstrated secretion of Collagen type II matrix around impregnated cells of the *in vitro*-cultured hybrid constructs. Similar to the Alcian blue staining results, Col2-stained matrix increased for both rounded and fibroblastic cells over time in culture (Fig. 10). At day 1 and 7, rounded and fibroblastic cells showed comparable Col2 matrix secretion. However, fibroblastic

cell hybrid constructs seemed to have larger and more continuous Col2-stained matrix than the rounded cells by day 14 of culture (Fig. 10D, E, I, J). The cells impregnated in the constructs also secreted some Collagen type X (Col10) matrix after long-term *in vitro* culture (Supplementary Fig. S1; Supplementary Data are available online at www.liebertpub.com/tec). In summary, these data demonstrate that hybrid constructs are permissive for chondrogenic differentiation and secretion of Collagen type II matrix by both rounded and fibroblastic cells.

Biofabrication of cartilage hybrid constructs can be scaled up successfully

To confirm that this biofabrication method can be scaled up to make biologically functional constructs with a thickness approximating that of mature cartilage, 6-layer constructs were printed, and the cell viability and matrix production were evaluated. For these experiments, the common chondrogenic cell line, ATDC5,^{56,57} was used. High cell viability and Alcian blue staining at days 14 and

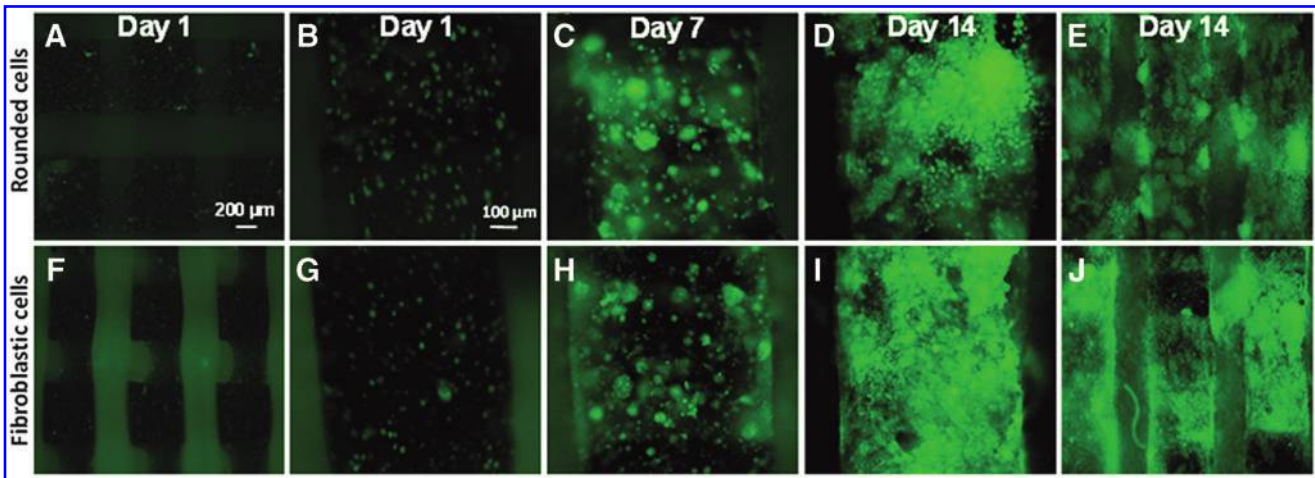


FIG. 10. Collagen type II (Col2) immunofluorescence staining illustrates increase of Col2-positive matrix over time in 3D hybrid constructs. Fluorescent images of constructs impregnated with rounded (A–E) and fibroblastic cells (F–J) at day 1 (A, B, F, G), day 7 (C, H), and day 14 (D, E, I, J). The same exposure time was used for (B–D, G–I) to illustrate relative increase in Col2 immunostaining during culture. Color images available online at www.liebertpub.com/tec

28 of culture demonstrated that this hybrid biofabrication method can be scaled up to create multilayer constructs that maintain high cell viability and secretion of GAGs (Fig. 11, and data not shown). Cross-section views further confirmed the biocompatibility of the PCL printing temperature. Similar to the two-layer hybrid constructs (Fig. 8A–G), uniform distribution of cells within the alginate throughout the thickness of six-layer constructs verified the integrity of the alginate hydrogel 3D structure during *in vitro* culture (Fig. 11). These results not only demonstrate the successful up-scaling of this biofabrication method but also illustrate its versatility on multiple cell sources.

Discussion

Identifying parameters of biofabrication that enable reproducible results, while ensuring biocompatibility, is critical to future clinical applications of tissue engineering. Recently, the sophisticated tissue-engineering strategy of 3D bioprinting live cells into hybrid constructs has been attracting more attention

since it can generate customized structural and biological functions. In addition, this biofabrication method is automated, hands free, and economical, showing promise to improve cartilage tissue regeneration and facilitate clinical translations. The feasibility of using 3D bioprinting for cartilage tissue engineering had been shown by limited studies,^{23–25} and this study confirmed and significantly expanded the promising potential of this technique.

Parameters of a hybrid biofabrication process that employs melt-dispensed PCL polymer and chondrocyte-impregnated alginate were identified to enable biocompatible impregnation of cells and allow maintenance of structural integrity of the construct. Throughout culture periods of 4 weeks, impregnated cells were distributed uniformly, and a high cell viability was observed (Figs. 7 and 8). Although PCL was dispensed at high temperatures, there was a relatively fast (within seconds) and large decrease of temperature at the surface of the dispensed PCL strand (Fig. 2), presumably because the small size of the strands accelerated the cooling process. The high observed cell viability during

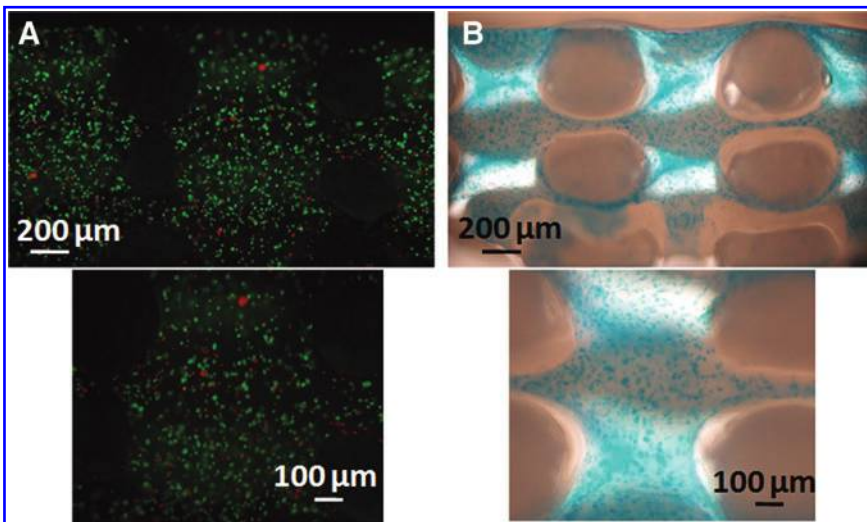


FIG. 11. Six-layer hybrid constructs with impregnated ATDC5 cells also demonstrate good biofunctionality. Cross-section views of six-layer constructs revealed promising biological performance by (A) live (green) and dead (red) cell viability assay, and (B) Alcian blue-positive matrix at day 14. Cross-section of the PCL strands and the outline of the transverse PCL strands that make the 0/90° pattern in the stacked layers are seen in (B). Color images available online at www.liebertpub.com/tec

biofabrication of hybrid constructs may result from this rapid cooling since there was no spatial correlation between dead cells and dispensed PCL (Figs. 7 and 11)

Reproducible and biocompatible 3D printing of structurally stable hydrogels remains a challenge. The PCL scaffold provides mechanical properties to the hybrid construct,²⁵ with the goal of withstanding loading of the joint after *in situ* implantation, yet still allowing some transfer of applied mechanical stimuli to the cells in the alginate. In the absence of any external loading, such as in the experiments reported in this study, the PCL scaffold likely does not affect the biological behavior of cells encapsulated in the alginate. The performance of the PCL scaffold in transferring customized mechanical stimuli (modulated by the PCL architectural design) to the cells in the alginate is recommended to be investigated in future studies.

Despite mechanical support from PCL, the alginate strands in hybrid constructs also need to exhibit some level of stability after fabrication to maintain the customized design properties. Cross-linking the hydrogel before dispensing can improve biofabrication,³⁸ but the cross-linking process is progressive, leading to changes in hydrogel viscosity over time. This introduces undesirable time-dependent variability to the fabrication process, making the precross-linking method less reproducible. The more common approach of using higher concentrations of alginate (e.g., 3.5–10%^{24,38,62}) also benefits its structural stability, but suffers from limitations on biocompatibility. Cells are subjected to an increased shear stress during printing,^{26,27} and increased alginate concentrations may provide a less favorable biological environment for some cells.^{24,28,29} In this study, suitable biofabrication parameters were identified to avoid these limitations. A combination of alginate processing temperature and initial viscosity was found to improve printability at low concentrations (2% and 2.5% w/w) without any precross-linking (Fig. 6). This finding should assist tissue-engineering strategies that require low hydrogel concentrations for biological reasons.⁶³

To evaluate the biological performance of hybrid constructs, two distinct cell populations isolated from embryonic chick cartilage were assayed for cell viability, proliferation, and secretion of cartilage ECM components during lengthy periods of *in vitro* culture. The rounded and fibroblastic cell populations were identified in 2D primary cultures based upon morphology (round vs. elongated) and adhesive affinity to the culture flask (floating/easily detached vs. firmly attached) (Fig. 4). After bioprinting into 3D hybrid constructs, these cell populations continued to demonstrate some differences (i.e., time course of proliferation and secretion of cartilage ECM) (Figs. 8–10), but they both showed high overall biological performance (Figs. 7–10).

Focusing first on similarities in the *in vitro* performance of two distinct cell populations in hybrid constructs, both rounded and fibroblastic cells displayed high viability and abundant secretion of cartilage ECM (Figs. 7, 9, and 10). The cell viability was over 80% for up to 14 days of culture. In addition, abundant Alcian blue staining and Col2 immunostaining in both cell populations (Figs. 9, 10) reflect secretion of the two major components of cartilage ECM, GAGs and Collagen type II,⁶¹ further demonstrating the promising biocompatibility of this 3D biofabrication method. While the majority of impregnated cells appear to maintain a nonhypertrophic cartilaginous phenotype throughout the

examined culture period, a few cells expressed Col10 after long culture time (Supplementary Fig. S1). The Col10 expression is characteristic of deep and calcified layers of articular cartilage,^{64–66} so future work must be done to regulate layer-specific gene expression in engineered cartilage constructs. These are critical results for therapeutic applications of cartilage tissue engineering since culturing tissue constructs *in vitro* for a period of time may allow cells to initiate lineage-specific (e.g., chondrocyte) cellular activities before *in vivo* implantation.^{34,67}

Differences in biological performance of the rounded and fibroblastic cells in hybrid constructs are presumed to rise from intrinsic differences between the two cell populations since similar results were obtained in many independent experiments. These results raise the general issue of the importance of selecting among alternative cell sources for tissue engineering applications. Rounded and fibroblastic cells showed differences in the timing of cell proliferation and secretion of cartilage ECM (Figs. 8–10). A dramatic increase in the proliferation of fibroblastic cells compared to rounded cells was observed at later time points of 3D hybrid construct culture (Fig. 8).

In addition, statistically larger regions of Alcian blue-stained matrix appeared in fibroblastic cells than in rounded cells at days 7 and 14 of culture (Fig. 9), and fibroblastic cell constructs appeared to contain larger areas of Col2-positive matrix than the rounded cells at day 14 of culture (Fig. 10). Together, these data suggest that fibroblastic cells secrete abundant cartilage ECM earlier than rounded cells, but they also maintain capacity for proliferation longer than the rounded cells. Both these features seem beneficial for therapeutic applications of cartilage tissue engineering and call for an understanding of the mechanistic basis for these observations.

Despite the fact that both rounded and fibroblastic cells were isolated from the same source (embryonic cartilage), we propose that differences in their biological performance in 3D hybrid constructs are explained by the idea that they are at different states of chondrocyte differentiation. Rounded cells have typical chondrocyte morphology,⁶⁸ suggesting that they may be differentiated chondrocytes. On the other hand, fibroblastic cells have a morphology that is typical of many cell types, including stem cells.⁶⁹ Given their origin from embryonic cartilage, the fibroblastic cells may be undifferentiated cartilage stem cells (chondroprogenitors) or dedifferentiated chondrocytes. While dedifferentiation of primary cells is common in 2D culture,^{70,71} two functional observations support the assertion that fibroblastic cells are cartilage stem cells.

Chondroprogenitor cells maintain the capacity for cell division,³⁶ and fibroblastic cells demonstrated an increased cell proliferation. In addition, the asymmetric division of progenitor cells gives rise to differentiated cells,^{36,72} and fibroblastic cells appeared to give rise to rounded cells during 2D culture (Fig. 4). Interestingly, when rounded cells were cultured in a 2D environment, some cells attached to the substrate and formed fibroblastic morphology (data not shown), indicating that some rounded cells still have the potential to dedifferentiate and attach to the tissue culture plate. A similar behavior of cartilage cells in 2D culture has also been observed in human,⁷³ murine,^{74,75} and chick^{76,77} primary embryonic chondrocytes. Moreover, the continued proliferation of the rounded cells in the 3D constructs (Fig. 8) suggests that they may not be fully matured postmitotic chondrocytes,

which have low proliferation capability.^{78,79} In fact, their proliferative capability is similar to transiently amplifying chondrocytes that are organized into columns of the developing growth plate.^{79,80} Finally, molecular data support the idea that rounded cells are chondrocytes and fibroblastic cells are chondroprogenitors (Fig. 5). qPCR analyses directly after 3D bioprinting showed that rounded cells had a significantly higher expression of *Col2a1*, a marker of differentiated chondrocytes,^{61,81,82} while fibroblastic cells expressed significantly higher levels of *Col1a2*, a marker of undifferentiated mesenchymal cells.^{83,84}

In total, these functional and molecular data suggest that chondroprogenitors may serve as a better cell source than differentiated chondrocytes in cartilage tissue engineering since they produce cartilage ECM quicker and proliferate more. Such speculation needs to be supported by rigorous molecular characterization (e.g., transcriptomics) and clonal cell analyses, but would inform a critical unresolved issue for therapeutic applications of cartilage tissue engineering. Which among the two common cell sources is best: chondroprogenitors from mesenchymal stem cells or primary chondrocytes isolated from differentiated cartilage^{36,85–88?}

To be clinically relevant, biofabrication methods must work with a variety of cell sources and also be capable of making constructs that match the size of the tissue to be replaced. The cartilage tissue engineering method developed in this study satisfied these objectives. Good biological performance in hybrid constructs was observed using three different cell types and sources: rounded and fibroblastic cells from primary embryonic chick cartilage, as well as a mammalian chondrocytic cell line, ATDC5. While these cells do not have direct application to large animal and human studies, the primary cell isolation method used in this study from embryonic chick is similar to that used to isolate primary chondrocytes from larger animals and human tissues.⁸⁹ Future applications of this hybrid biofabrication method should be explored using primary chondrocytes and mesenchymal stem cells from adult tissues.

Furthermore, the hybrid biofabrication method demonstrated a good performance when scaled up from two-layer (480 μ m) to six-layer (1.44 mm) constructs (Fig. 11). These six-layer constructs approximate the average thickness of human articular cartilage (e.g.,⁵⁵). Future applications of this hybrid fabrication method may improve engineering of cartilage and other tissues. Complex structural and biological properties could be designed into constructs that mimic the zonal characteristics of articular cartilage.^{21,31} Such biomimetic tissue constructs may promote more natural ECM formation.^{90,91}

In addition to cartilage tissue engineering, the developed biofabrication method could improve functionality of many different soft- and hard-engineered tissues (such as tendon, ligament, bone, and tooth) that require synergistic components with customized properties.^{92,93} Advanced biofabrication technologies build the foundations for hands-free, automated, aseptic, and economic tissue engineering methodologies that are required for large-scale clinical trials.^{94–96}

Conclusion

In this study, a 3D printing-based biofabrication technique was developed successfully for making custom-designed hybrid constructs from polymer and cell-impregnated hydrogel.

Demonstrating the potential for advanced cartilage tissue engineering, this hybrid biofabrication enabled good biological performance (viability, proliferation, and cartilage ECM secretion) of three different cell types (two primary embryonic cell populations and an established chondrocyte line). Statistically significant differences in biological performance of two morphologically distinct cell populations isolated from embryonic chick cartilage were discussed in relation to the strategy of using differentiated vs. progenitor cells in tissue engineering. The hybrid biofabrication method described in this study can be used to develop sophisticated biomimetic tissue constructs with more complicated structures and functions.

Acknowledgment

This work was supported by a Saskatchewan Health Research Foundation (SHRF) Phase III Research Group grant to XBC, WK, and BFE, Natural Sciences and Engineering Research Council (NSERC) Discovery Grants to XBC and BFE, a SHRF Establishment Grant to BFE, a Canadian Institutes of Health Research (CIHR) New Investigator Award to BFE, and the CIHR-Training in Health Research Using Synchrotron Techniques (THRUST) program. Zohreh Izadifar is a fellow in the Canadian Institute of Health Research Training grant in Health Research Using Synchrotron Techniques (CIHR-THRUST).

Disclosure Statement

The authors have no conflicts of interest to declare.

References

1. Makris, E.A., Gomoll, A.H., Malizos, K.N., Hu, J.C., and Athanasiou, K.A. Repair and tissue engineering techniques for articular cartilage. *Nat Rev Rheumatol* **11**, 21, 2015.
2. Hunziker, E.B., Lippuner, K., and Shintani, N. How best to preserve and reveal the structural intricacies of cartilaginous tissue. *Matrix Biol* **39**, 33, 2014.
3. Athanasiou, K.A., Darling, E.M., and Hu, J. Articular cartilage tissue engineering. In: Athanasiou, K.A., and Leach, J.K., eds. *Synthesis Lectures on Tissue Engineering*. San Rafael, CA: Morgan & Claypool, 2009, p 182.
4. Bian, L., *et al.* Dynamic mechanical loading enhances functional properties of tissue-engineered cartilage using mature canine chondrocytes. *Tissue Eng Part A* **16**, 1781, 2010.
5. Kisiday, J.D., Jin, M., DiMicco, M.A., Kurz, B., and Grodzinsky, A.J. Effects of dynamic compressive loading on chondrocyte biosynthesis in self-assembling peptide scaffolds. *J Biomech* **37**, 595, 2004.
6. Kawanishi, M., *et al.* Redifferentiation of dedifferentiated bovine articular chondrocytes enhanced by cyclic hydrostatic pressure under a gas-controlled system. *Tissue Eng* **13**, 957, 2007.
7. Poole, A.R., *et al.* Composition and structure of articular cartilage: a template for tissue repair. *Clin Orthop Relat Res* **691Suppl**, S26, 2001.
8. Chang, C.-H., Lin, F.-H., Kuo, T.-F., and Liu, H.-C. Cartilage tissue engineering. *Biomed Eng (Singapore)* **17**, 61, 2005.
9. Bryant, S.J., and Anseth, K.S. Hydrogel properties influence ECM production by chondrocytes photoencapsulated in poly(ethylene glycol) hydrogels. *J Biomed Mater Res* **59**, 63, 2002.

10. Rahfoth, B., *et al.* Transplantation of allograft chondrocytes embedded in agarose gel into cartilage defects of rabbits. *Osteoarthritis Cartilage* **6**, 50, 1998.
11. Elisseeff, J.H., Yamada, Y., and Langer, R. Biomaterials for tissue engineering. In: K.U. Lewandrowski *et al.* eds. *Tissue Engineering and Biodegradable Equivalents: Scientific and Clinical Applications*. New York, NY: Marcel Dekker, Inc., 2002, p 23.
12. Li, W.J., Laurencin, C.T., Caterson, E.J., Tuan, R.S., and Ko, F.K. Electrospun nanofibrous structure: a novel scaffold for tissue engineering. *J Biomed Mater Res* **60**, 613, 2002.
13. Sechriest, V.F., *et al.* GAG-augmented polysaccharide hydrogel: a novel biocompatible and biodegradable material to support chondrogenesis. *J Biomed Mater Res* **49**, 534, 2000.
14. Puppi, D., Chiellini, F., Piras, A.M., and Chiellini, E. Polymeric materials for bone and cartilage repair. *Prog Polym Sci* **35**, 403, 2010.
15. Moutos, F.T. *Biomimetic Composite Scaffold for the Functional Tissue Engineering of Articular Cartilage* [Ph.D. thesis]. Durham, NC: Duke University, 2009.
16. Xu, T., *et al.* Hybrid printing of mechanically and biologically improved constructs for cartilage tissue engineering applications. *Biofabrication* **5**, 015001, 2013.
17. Jung, Y., Kim, S.H., Kim, Y.H., and Kim, S.H. The effect of hybridization of hydrogels and poly(L-lactide-co-epsilon-caprolactone) scaffolds on cartilage tissue engineering. *J Biomater Sci Polym Ed* **21**, 581, 2010.
18. Tanaka, Y., *et al.* The optimization of porous polymeric scaffolds for chondrocyte/atelocollagen based tissue-engineered cartilage. *Biomaterials* **31**, 4506, 2010.
19. Schagemann, J.C., *et al.* Poly-epsilon-caprolactone/gel hybrid scaffolds for cartilage tissue engineering. *J Biomed Mater Res A* **93**, 454, 2010.
20. Kawazoe, N., Inoue, C., Tateishi, T., and Chen, G. A cell leakproof PLGA-collagen hybrid scaffold for cartilage tissue engineering. *Biotechnol Prog* **26**, 819, 2010.
21. Izadifar, Z., Chen, X., and Kulyk, W. Strategic design and fabrication of engineered scaffolds for articular cartilage repair. *J Funct Biomater* **3**, 799, 2012.
22. Pfister, A., *et al.* Biofunctional rapid prototyping for tissue-engineering applications: 3D biplotting versus 3D printing. *J Polym Sci A Polym Chem* **42**, 624, 2004.
23. Pati, F., *et al.* Printing three-dimensional tissue analogues with decellularized extracellular matrix bioink. *Nat Commun* **5**, 3935, 2014.
24. Kundu, J., Shim, J.H., Jang, J., Kim, S.W., and Cho, D.W. An additive manufacturing-based PCL-alginate-chondrocyte bioprinted scaffold for cartilage tissue engineering. *J Tissue Eng Regen Med* **9**, 1286, 2015.
25. Schuurman, W., *et al.* Bioprinting of hybrid tissue constructs with tailorable mechanical properties. *Biofabrication* **3**, 021001, 2011.
26. Li, M., Tian, X., Zhu, N., Schreyer, D.J., and Chen, X. Modeling process-induced cell damage in the biodepositing process. *Tissue Eng Part C Methods* **16**, 533, 2010.
27. Nair, K., Yan, K., and Sun, W. A Multi-level numerical model for quantifying cell deformation in impregnated alginate structures. *J Mech Mater Struct* **2**, 1121, 2007.
28. Bohari, S.P., Hukins, D.W., and Grover, L.M. Effect of calcium alginate concentration on viability and proliferation of encapsulated fibroblasts. *Biomed Mater Eng* **21**, 159, 2011.
29. Kong, H.J., Smith, M.K., and Mooney, D.J. Designing alginate hydrogels to maintain viability of immobilized cells. *Biomaterials* **24**, 4023, 2003.
30. Maher, P.S., Keatch, R.P., Donnelly, K., Mackay, R.E., and Paxton, J.Z. Construction of 3D biological matrices using rapid prototyping technology. *Rapid Prototyp J* **15**, 2009.
31. Klein, T.J., Malda, J., Sah, R.L., and Huttmacher, D.W. Tissue engineering of articular cartilage with biomimetic zones. *Tissue Eng Part B Rev* **15**, 143, 2009.
32. Chung, C., and Burdick, J.A. Engineering cartilage tissue. *Adv Drug Deliv Rev* **60**, 243, 2008.
33. Darling, E.M., and Athanasiou, K.A. Rapid phenotypic changes in passaged articular chondrocyte subpopulations. *J Orthop Res* **23**, 425, 2005.
34. Kock, L., van Donkelaar, C.C., and Ito, K. Tissue engineering of functional articular cartilage: the current status. *Cell Tissue Res* **347**, 613, 2012.
35. Discher, D.E., Mooney, D.J., and Zandstra, P.W. Growth factors, matrices, and forces combine and control stem cells. *Science* **324**, 1673, 2009.
36. O'Sullivan, J., D'Arcy, S., Barry, F.P., Murphy, J.M., and Coleman, C.M. Mesenchymal chondrogenitor cell origin and therapeutic potential. *Stem Cell Res Ther* **2**, 8, 2011.
37. Li, M., Tian, X., Schreyer, D.J., and Chen, X. Effect of needle geometry on flow rate and cell damage in the dispensing-based biofabrication process. *Biotechnol Prog* **27**, 1777, 2011.
38. Lee, H., Ahn, S., Bonassar, L.J., and Kim, G. Cell(MC3T3-E1)-printed poly(-caprolactone)/alginate hybrid scaffolds for tissue regeneration. *Macromol Rapid Commun* **34**, 142, 2013.
39. Meier, S., and Solursh, M. Ultrastructural analysis of the effect of ascorbic acid on secretion and assembly of extracellular matrix by cultured chick embryo chondrocytes. *J Ultrastruct Res* **65**, 48, 1978.
40. Thomas, J.T., and Grant, M.E. Cartilage proteoglycan aggregate and fibronectin can modulate the expression of type X collagen by embryonic chick chondrocytes cultured in collagen gels. *Biosci Rep* **8**, 163, 1988.
41. Farjanel, J., Schurmann, G., and Bruckner, P. Contacts with fibrils containing collagen I, but not collagens II, IX, and XI, can destabilize the cartilage phenotype of chondrocytes. *Osteoarthritis Cartilage* **9 Suppl A**, S55, 2001.
42. Walker, E.A., Verner, A., Flannery, C.R., and Archer, C.W. Cellular responses of embryonic hyaline cartilage to experimental wounding *in vitro*. *J Orthop Res* **18**, 25, 2000.
43. Hirsch, M.S., and Svoboda, K.H. Establishment of a whole-chick sternum model that recapitulates normal cartilage development. *Biotechniques* **24**, 632, 1998.
44. Huang, X., Zhang, Y., Donahue, H.J., and Lowe, T.L. Porous thermoresponsive-co-biodegradable hydrogels as tissue-engineering scaffolds for 3-dimensional *in vitro* culture of chondrocytes. *Tissue Eng* **13**, 2645, 2007.
45. Zhang, Z., McCaffery, J.M., Spencer, R.G., and Franco-mano, C.A. Growth and integration of neocartilage with native cartilage *in vitro*. *J Orthop Res* **23**, 433, 2005.
46. Zhang, Z., McCaffery, J.M., Spencer, R.G., and Franco-mano, C.A. Hyaline cartilage engineered by chondrocytes in pellet culture: histological, immunohistochemical and ultrastructural analysis in comparison with cartilage explants. *J Anat* **205**, 229, 2004.
47. Giroto, D., *et al.* Tissue-specific gene expression in chondrocytes grown on three-dimensional hyaluronic acid scaffolds. *Biomaterials* **24**, 3265, 2003.

48. Mayne, R., Vail, M.S., Mayne, P.M., and Miller, E.J. Changes in type of collagen synthesized as clones of chick chondrocytes grow and eventually lose division capacity. *Proc Natl Acad Sci USA* **73**, 1674, 1976.
49. von der Mark, K., Gauss, V., von der Mark, H., and Müller, P. Relationship between cell shape and type of collagen synthesized as chondrocytes lose their cartilage phenotype in culture. *Nature* **267**, 531, 1977.
50. Tschan, T., *et al.* Resting chondrocytes in culture survive without growth factors, but are sensitive to toxic oxygen metabolites. *J Cell Biol* **111**, 257, 1990.
51. Glaser, J.H., and Conrad, H.E. Properties of chick embryo chondrocytes grown in serum-free medium. *J Biol Chem* **259**, 6766, 1984.
52. Capasso, O., *et al.* The culture of chick embryo chondrocytes and the control of their differentiated functions *in vitro*. I. Characterization of the chondrocyte-specific phenotypes. *Exp Cell Res* **142**, 197, 1982.
53. Bounelis, P., and Daniel, J.C. Preparation of primary cultures of embryonic chick chondrocytes in agarose. *J Tissue Culture Methods* **7**, 111, 1982.
54. Eames, B.F., and Helms, J.A. Conserved molecular program regulating cranial and appendicular skeletogenesis. *Dev Dyn* **231**, 4, 2004.
55. Frisbie, D.D., Cross, M.W., and McIlwraith, C.W. A comparative study of articular cartilage thickness in the stifle of animal species used in human pre-clinical studies compared to articular cartilage thickness in the human knee. *Vet Comp Orthop Traumatol* **19**, 142, 2006.
56. Kwon, H.J., *et al.* *In vitro* differentiation of chondrogenic ATDC5 cells is enhanced by culturing on synthetic hydrogels with various charge densities. *Acta Biomater* **6**, 494, 2010.
57. Tare, R.S., Howard, D., Pound, J.C., Roach, H.I., and Orfello, R.O. Tissue engineering strategies for cartilage generation—micromass and three dimensional cultures using human chondrocytes and a continuous cell line. *Biochem Biophys Res Commun* **333**, 609, 2005.
58. Schneider, C.A., Rasband, W.S., Eliceiri, K.W. “NIH Image to ImageJ: 25 years of image analysis”. *Nature Methods* **9**, 671–675, 2012.
59. Radonic, A., *et al.* Guideline to reference gene selection for quantitative real-time PCR. *Biochem Biophys Res Commun* **313**, 856, 2004.
60. Livak, K.J., and Schmittgen, T.D. Analysis of relative gene expression data using real-time quantitative PCR and the 2(-Delta Delta C(T)) Method. *Methods* **25**, 402, 2001.
61. Eames, B.F., de la Fuente, L., and Helms, J.A. Molecular ontogeny of the skeleton. *Birth Defects Res C Embryo Today* **69**, 93, 2003.
62. Fedorovich, N.E., *et al.* Biofabrication of osteochondral tissue equivalents by printing topologically defined, cell-laden hydrogel scaffolds. *Tissue Eng Part C Methods* **18**, 33, 2012.
63. Khalil, S., and Sun, W. Bioprinting endothelial cells with alginate for 3D tissue constructs. *J Biomech Eng* **131**, 111002, 2009.
64. Kirsch, T., and von der Mark, K. Isolation of human type X collagen and immunolocalization in fetal human cartilage. *Eur J Biochem* **196**, 575, 1991.
65. Eerola, I., *et al.* Type X collagen, a natural component of mouse articular cartilage: association with growth, aging, and osteoarthritis. *Arthritis Rheum* **41**, 1287, 1998.
66. Reichenberger, E., Aigner, T., von der Mark, K., Stoss, H., and Bertling, W. *In situ* hybridization studies on the expression of type X collagen in fetal human cartilage. *Dev Biol* **148**, 562, 1991.
67. Deponti, D., *et al.* Fibrin-based model for cartilage regeneration: tissue maturation from *in vitro* to *in vivo*. *Tissue Eng Part A* **18**, 1109, 2012.
68. Glattauer, V., *et al.* Direct use of resorbable collagen-based beads for cell delivery in tissue engineering and cell therapy applications. In: Eberli, D., ed. *Regenerative Medicine and Tissue Engineering—Cells and Biomaterials*. Croatia, European Union: InTech, 2011.
69. Beyer Nardi, N., and da Silva Meirelles, L. Mesenchymal stem cells: isolation, *in vitro* expansion and characterization. *Handb Exp Pharmacol* **174**, 249, 2006.
70. Benya, P.D., Padilla, S.R., and Nimni, M.E. Independent regulation of collagen types by chondrocytes during the loss of differentiated function in culture. *Cell* **15**, 1313, 1978.
71. Elimä, K., and Vuorio, E. Expression of mRNAs for collagens and other matrix components in dedifferentiating and redifferentiating human chondrocytes in culture. *FEBS Lett* **258**, 195, 1989.
72. Schreibman, M. *The Endocrinology of Growth, Development, and Metabolism in Vertebrates*. San Diego, CA: Academic Press, Inc., 2012.
73. Stokes, D.G., *et al.* Assessment of the gene expression profile of differentiated and dedifferentiated human fetal chondrocytes by microarray analysis. *Arthritis Rheum* **46**, 404, 2002.
74. Mirando, A.J., Dong, Y., Kim, J., and Hilton, M.J. *T Skeletal Development and Repair, Methods in Molecular Biology*, New York, Heidelberg, Dordrecht, London: Springer. Vol. 1130, 2014, pp. 267–277.
75. Sautier, J.M., Nefussi, J.R., and Forest, N. *In vitro* differentiation and mineralization of cartilaginous nodules from enzymatically released rat nasal cartilage cells. *Biol Cell* **78**, 181, 1993.
76. Yasumoto, S., Kondo, S., and Kato, Y. Growth and differentiation of primary chick embryonic chondrocytes on agar plates. *Jpn J Exp Med* **50**, 221, 1980.
77. Guo, J.F., Jourdan, G.W., and MacCallum, D.K. Culture and growth characteristics of chondrocytes encapsulated in alginate beads. *Connect Tissue Res* **19**, 277, 1989.
78. Zhang, J., *et al.* The influence of scaffold microstructure on chondrogenic differentiation of mesenchymal stem cells. *Biomed Mater* **9**, 035011, 2014.
79. St-Jacques, B., Hammerschmidt, M., and McMahon, A.P. Indian hedgehog signaling regulates proliferation and differentiation of chondrocytes and is essential for bone formation. *Genes Dev* **13**, 2072, 1999.
80. Lanza, R., *et al.* *Handbook of Stem Cells, Two-Volume Set: Volume 1-Embryonic Stem Cells; Volume 2-Adult & Fetal Stem Cells*. Cambridge, MA: Academic Press, 2004.
81. Eames, B.F., *et al.* Skeletogenesis in the swell shark *Cephaloscyllium ventriosum*. *J Anat* **210**, 542, 2007.
82. Eames, B.F., Amores, A., Yan, Y.L., and Postlethwait, J.H. Evolution of the osteoblast: skeletogenesis in gar and zebrafish. *BMC Evol Biol* **12**, 27, 2012.
83. Zhang, H., Kay, A., Forsyth, N.R., Liu, K.K., and El Haj, A.J. Gene expression of single human mesenchymal stem cell in response to fluid shear. *J Tissue Eng* **3**, 2041731412451988, 2012.
84. Kulterer, B., *et al.* Gene expression profiling of human mesenchymal stem cells derived from bone marrow during expansion and osteoblast differentiation. *BMC Genomics* **8**, 70, 2007.

85. Arai, F., Ohneda, O., Miyamoto, T., Zhang, X.Q., and Suda, T. Mesenchymal stem cells in perichondrium express activated leukocyte cell adhesion molecule and participate in bone marrow formation. *J Exp Med* **195**, 1549, 2002.
86. English, A., *et al.* A comparative assessment of cartilage and joint fat pad as a potential source of cells for autologous therapy development in knee osteoarthritis. *Rheumatology* **46**, 1676, 2007.
87. De Ugarte, D.A., *et al.* Comparison of multi-lineage cells from human adipose tissue and bone marrow. *Cells Tissues Organs* **174**, 101, 2003.
88. Friedenstein, A., Piatetzky-Shapiro, I., and Petrakova, K. Osteogenesis in transplants of bone marrow cells. *J Embryol Exp Morphol* **16**, 381, 1966.
89. Tew, S.R., Murdoch, A.D., Rauchenberg, R.P., and Hardingham, T.E. Cellular methods in cartilage research: primary human chondrocytes in culture and chondrogenesis in human bone marrow stem cells. *Methods* **45**, 2, 2008.
90. McCullen, S.D., Autefage, H., Callanan, A., Gentleman, E., and Stevens, M.M. Anisotropic fibrous scaffolds for articular cartilage regeneration. *Tissue Eng Part A* **18**, 2073, 2012.
91. Nguyen, L.H., Kudva, A.K., Saxena, N.S., and Roy, K. Engineering articular cartilage with spatially-varying matrix composition and mechanical properties from a single stem cell population using a multi-layered hydrogel. *Biomaterials* **32**, 6946, 2011.
92. Longo, U.G., Lamberti, A., Maffulli, N., and Denaro, V. Tendon augmentation grafts: a systematic review. *Br Med Bull* **94**, 165, 2010.
93. Park, C.H., *et al.* Biomimetic hybrid scaffolds for engineering human tooth-ligament interfaces. *Biomaterials* **31**, 5945, 2010.
94. Mironov, V., Kasyanov, V., and Markwald, R.R. Organ printing: from bioprinter to organ biofabrication line. *Curr Opin Biotechnol* **22**, 667, 2011.
95. Mironov, V., *et al.* Biofabrication: a 21st century manufacturing paradigm. *Biofabrication* **1**, 022001, 2009.
96. Cohen, D.L., Malone, E., Lipson, H., and Bonassar, L.J. Direct freeform fabrication of seeded hydrogels in arbitrary geometries. *Tissue Eng* **12**, 1325, 2006.

Address correspondence to:

B. Frank Eames, PhD

Department of Anatomy and Cell Biology

University of Saskatchewan

107 Wiggins Road

Saskatoon, SK, S7N 5E5

Canada

E-mail: b.frank@usask.ca

Received: June 30, 2015

Accepted: November 20, 2015

Online Publication Date: December 30, 2015